MJFAS
Malaysian Journal of Fundamental and Applied Sciences

Aziz *et al.* | Malaysian Journal of Fundamental and Applied Sciences, Vol. 18 (2022) 383-392

RESEARCH ARTICLE

Structural, Morphological and Optical Properties of Zinc Oxide Nanorods prepared by ZnO Seed Layer Annealed at Different Oxidation Temperature

Muhammad Safwan Abd Aziz[a,b,c,*], Mohd Shahril Salleh[b], Ganesan Krishnan[a,b], Nandang Mufti[d,e], M. F. Omar[b], S. W. Harun[c]

[a] Laser Centre, Ibnu Sina Institute for Scientific and Industrial Research, Universiti Teknologi Malaysia (UTM), 81310 Skudai, Johor, Malaysia; [b] Department of Physics, Faculty of Science, Universiti Teknologi Malaysia (UTM), 81310 Skudai, Johor, Malaysia; [c] Photonics Engineering Laboratory, Department of Electrical Engineering, Faculty of Engineering, University of Malaya, 50603, Kuala Lumpur, Malaysia; [d] Department of Physics, Faculty of Mathematics and Natural Sciences, State University of Malang, Jl. Semarang 5, Malang, 65145, Indonesia; [e] Center of Advanced Materials for Renewable Energy, State University of Malang, Jl. Semarang 5, Malang, 65145, Indonesia

Abstract In this work, zinc oxide (ZnO) nanorods structure in the form of thin film have been grown on soda-lime glass (SLG) substrate incorporating two simple steps. Firstly, ZnO seed layer was pre-deposited onto the SLG substrate by the thermal evaporation method. During this process, the oxidation temperatures were varied in the range of 450 °C to 650 °C annealed for 3 hours. Then, the nanorods structure were grown on the surface of the seed layer by sol-gel immersion method with the use of zinc nitrate hexahydrate ($Zn(NO_3)_2 \cdot 6H_2O$) and hexamethylenetetramine (HMT) in deionized (DI) water. The optical, structural and morphological properties at different oxidation temperatures were studied using UV-Vis-NIR spectroscopy, X-ray diffraction (XRD) and Field-enhanced Scanning Electron Microscopy (FeSEM). The surface morphology results revealed the formation of hexagonal shaped ZnO on top of the seed layer as a result of heterogeneous nucleation. X-ray diffraction results show that the c-axis orientation became more prominent while the optical band gap of ZnO thin films decreases from 3.31 eV to 3.14 eV as the annealing temperature increased respectively. It is shown that the size and alignment of ZnO NRs are greatly affected by the pre-deposition annealed temperature of the ZnO seed layer on the surface of SLG substrate.

Keywords: Zinc Oxide, Nanorods, Oxidation temperature, sol-gel.

***For correspondence:**
safwanaziz@utm.my

Received: 21 Dec 2021
Accepted: 21 April 2022

Introduction

Zinc oxide (ZnO) is considered one of the unique materials that have been under intense study in the field of science and technology. This metal oxide offers several remarkable properties such as facile synthesis, high surface to volume ratio, relatively low toxicity as well as excellent chemical and mechanical stability despite being abundant in nature [1]. ZnO is classified as a semiconductor in group II-VI having a wide and direct bandgap of 3.37 eV with a large exciton binding energy of 60 meV which make it find its way in a broad range of applications such as in optoelectronics [2-4], sensors [5, 6] and biomedical applications [7-9]. Recently, ZnO in its one-dimensional (1D) form such as nanorod structure

has attracted considerable attention among researchers. Compared to its bulk or two-dimensional (2D) counterparts, 1D semiconducting ZnO nanostructures exhibit significant improvement especially in photoelectric properties including strong optical absorption, multiple light confinement as well as low energy loss of the light-generated carrier [10]. To date, numerous attempts have been made to synthesize highly crystalline ZnO nanorods structure with good absorption in the UV region through chemical vapor deposition [11], thermal evaporation [12], hydrothermal [13], atomic layer deposition [14], and microwave-assisted technique [15]. Despite versatile synthesis techniques, the most unique property of ZnO itself lies in the possibility of tailoring ZnO nanostructure with different morphologies and sizes by merely changing the critical parameters during the process.

For instance, it has been reported that the deposition parameter of the ZnO seed layer heavily affects the growth mechanism of ZnO nanorods on a glass substrate [16]. ZnO seed layer plays an essential role in reducing the lattice mismatch between ZnO NRs and Si substrate as well as assisting the heterogeneous nucleation of ZnO on the surface of the thin film. Therefore, careful examination on ZnO seed layer inherent properties towards the growth mechanism of ZnO in nanostructure form is relatively important to gain a better understanding of the process. In this work, the influence of pre-annealing temperature of ZnO seed layer towards the final optical, structural, and morphological properties of ZnO NR by sol-gel immersion technique is reported.

Materials and Methods

Zn thin film deposition by thermal evaporation method

Thermal evaporation process for depositing Zn thin films was carried out by using ZHD300 High Vacuum Thermal Evaporator, while zinc target (0.8 g, 99.9% purity) was used as vapor source for depositing the Zn thin films. Prior of this processes, soda-lime glass substrates (2 cm x 2 cm) were ultrasonically cleaned at 50 °C with soap, methanol and deionized water, each for 10 minutes and finally dried in the ambient air. The target was placed on a molybdenum boat, while glass substrates were held by stainless steel substrate holder, 25 cm above the Zn target. The deposition chamber then evacuated using a combination of mechanical and molecular pumps to a base pressure 9.0×10^{-4} Pa. Zn target was heated for about 10 minutes by applying current to the molybdenum boat, and the current slowly increased to 85 A. Afterwards, the deposition process took about 25 minutes at working pressure 1.4×10^{-3} Pa. In order to complete the formation of the seed layer, oxidation process with certain annealing temperatures were performed and transformed Zn to ZnO seed layer.

ZnO thin film prepared by tube furnace

Subsequently, successful deposited Zn thin film were annealed in GSL-1100X Tube Furnace for oxidation process. Three different temperatures were chosen for this step, which are 450 °C, 550 °C and 650 °C. In this process, Zn thin film was fixed in the middle of an alumina combustion boat, later inserted into the heating region of the tube furnace. Ar^2 gas was purged and flushed out for three times to ensure that no other gases reside in the tube. Later, O^2 gas was flowed and maintained at 5×10^4 Pa. Zn thin films were then annealed at three different temperatures, which are 450 °C, 550 °C and 650 °C. For simplification, samples are specified as S1 (450 °C), S2 (550 °C) and S3 (650 °C). For all annealing temperatures, three-step temperature approach were applied, as shown in Figure 1. First, Zn thin films were annealed at 10 °C per minute from room temperature to 300 °C in the first-step of the annealing process. The heating rate then was slowed down to 5 °C per minute until it reached second-step, which are 400 °C (S1), 500 °C (S2) and 600 °C (S3). Later, these temperatures were increased 50 °C higher to the third-step of the annealing process at ramping rate 0.8 °C per minute and maintained for 30 minutes. Afterwards, Zn thin films were cooled down back to second-step temperature in 30 minutes, which later cooled down naturally to the room temperature. Fabricated ZnO thin films were used as seeded catalysts, for synthesizing the ZnO nanorods.

ZnO nanorods growth by sol-gel immersion method

The growth of ZnO nanorods was carried out by sol-gel immersion method. In a typical process, 0.9468 g of zinc nitrate hexahydrate ($Zn(NO_3)_2.6H_2O$) and 0.70093 g of hexamethylenetetramine (HMT, $H_2NCH_2CH_2OH$) was diluted in 100 mL of deionized water in a 250 mL Pyrex beaker. Later, the solution was sonicated at 50°C for 30 minutes in ultrasonic water bath. Subsequently, sonicated solution was aged and stirred for 3 hours at room temperature. Fabricated ZnO thin films then placed horizontally, face up, at the bottom of Schott bottle, which later poured with the sonicated and aged solution. Afterwards, the capped Schott bottle was immersed for 4 hours in a 95°C water bath. Finally, these ZnO nanorods were cleaned with deionized water and allowed to dry in ambient air.

Characterization methods

Formation of Zn thin film to nanorods was studied. For optical properties, the absorption spectrum of ZnO thin films and nanorods were recorded on UV-Vis-NIR UV-3600 Plus Series Spectrometer. The structural properties of all samples were characterized by Rigaku Smartlab X-Ray Diffractometer with Cu Kα radiation (40kV, 20mA, λ = 0.15406 nm). Morphologies of samples were analyzed using Hitachi SU8020 Field Emission Scanning Electron Microscope (FESEM) with accelerating voltage of 20 kV respectively.

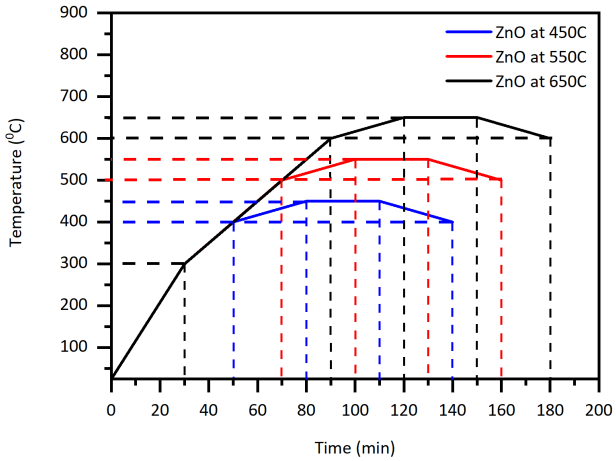

Figure 1. Three-step temperature approach for oxidation process of Zn thin film

Results and Discussion

Characterization of Zn Thin film as Seed Layer

XRD pattern of Zn thin film is determined by X-Ray Diffractrometer and shown in Figure 2, corresponding to JCPDS# 04-0831. Graph intensity versus 2θ shows major peaks of Zn thin film at 36.30° (002), 38.99° (100), 43.23° (101), 54.34° (102), 70.06° (103) and 70.66° (110). Peak with (101) plane at 43.23° has the highest intensity with full width half maximum (FWHM) value 0.3512°, which shows that Zn thin film deposited has high crystallinity. Furthermore, no other peak was found, showing that deposited thin film is high purity Zn. For surface morphology of Zn thin film, their micrographs were captured by FESEM with different magnification, and shown in Figure 3. In Figure 3 (a), it is illustrated that deposited layer surface is smooth and uniform. It is also clear that the film has elongated, graded and corner-shape grains, length between 407 nm to 1.53 μm, as shown in Figure 3 (b). From both characterization methods, it can be considered that high purity with good crystallinity of Zn thin film is successfully deposited and ready for the annealing process in order to transform it to ZnO thin film.

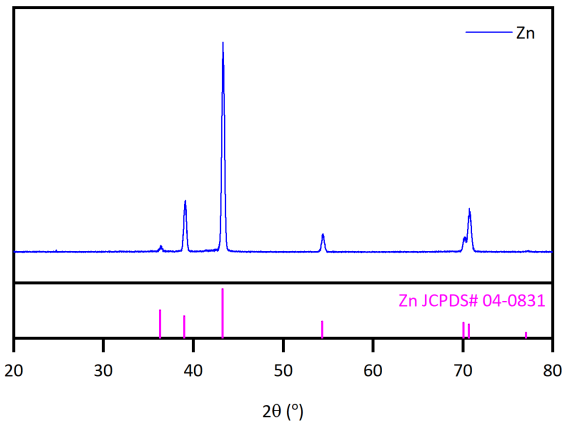

Figure 2. XRD pattern of Zn thin film deposited by thermal evaporation method 25 minutes at working pressure 1.4 x 10^{-3} Pa.

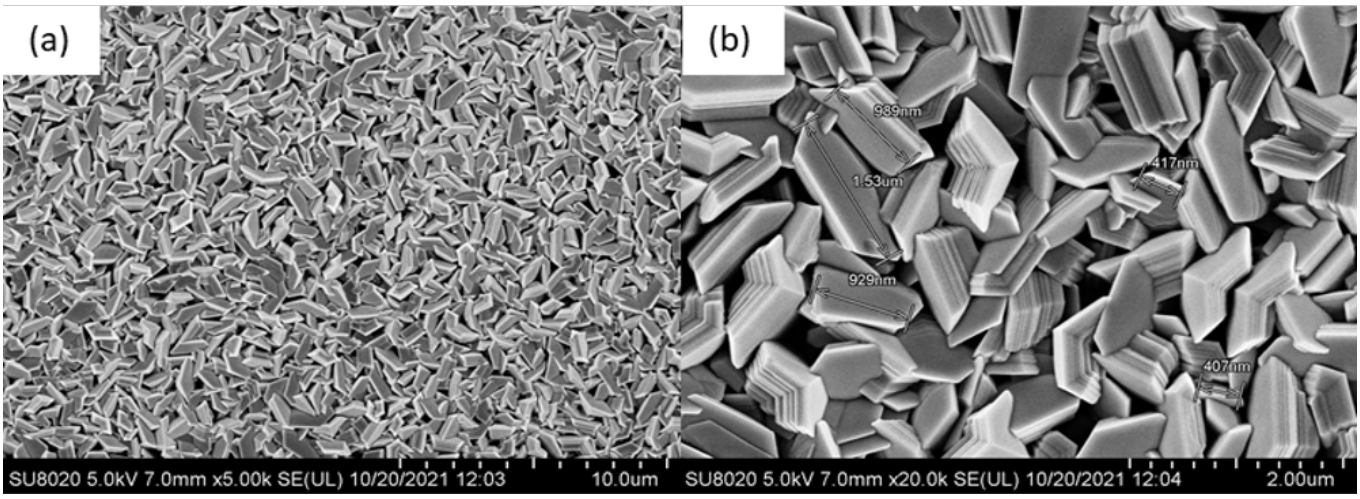

Figure 3. Zn thin film micrographs in (a) 5k and (b) 20k magnification

Optical, Structural and Morphological Analysis of ZnO Thin film

Absorbance spectrum of ZnO seed layer were characterized by UV-Vis-NIR Spectrometer as shown in Figure 4 (a) in the range of 200 to 800 nm of wavelength. Result shows that all thin film samples have high ultraviolet absorbance properties at wavelengths below 400 nm. Furthermore, the absorbance edges of these ZnO thin films are in range 400 to 450 nm of wavelength.The direct energy bandgap, E_g, of ZnO thin film samples can be determined by analysing the optical data with the expression for the optical absorbance, α, and photon energy, $h\upsilon$, as expressed in Tauc relation formula (1):

$$\alpha h\upsilon = C(h\upsilon - E_g)^n \quad (1)$$

Where C is constant, n constant is ½ for direct transition, h is the Planck constant and υ is the frequency, as:

$$h\upsilon = \frac{1240}{\lambda} \quad (2)$$

A graph between $(\alpha h\upsilon)^2$ versus $h\upsilon$ was plotted, and a straight line is plotted from the graph which intersects the x-axis. Energy bandgap of each samples is the x coordinate when the y coordinate is zero. Figure 4 (b) shows the energy bandgap for S1_TF, S2_TF and S3_TF. As shown in the figure, the energy bandgaps of these thin films are inversely proportional with the oxidation temperatures. This phenomenon might be caused by improved crystalline structure of these thin films when the oxidation temperature is increased. At low temperatures, lowest states in conduction bands are localized caused by disorder arrangements of thin film growth. As the amorphous nature of ZnO phase is increases, extended localization in valence and conduction band also increases. Nevertheless, the amorphous phase is decreases as the annealing temperature increases, which later caused the decrement of energy bandgap [17].

XRD pattern of ZnO seed layers is shown in Figure 5. The results revealed peaks located at 31.77° (100), 34.42° (002), 36.25° (101), 47.53° (102), 56.59° (110), 62.85° (103), 66.37° (200), 67.94° (112), 69.08° (201), 72.56° (004) and 76.95° (202), corresponded to characteristic peaks of ZnO (JCPDS# 79-2205). However, for S1_TF, Zn peaks were found at 38.99° (100) and 43.23° (101), associated to JCPDS# 04-0831, showing there are unreacted Zn that are not oxidized.

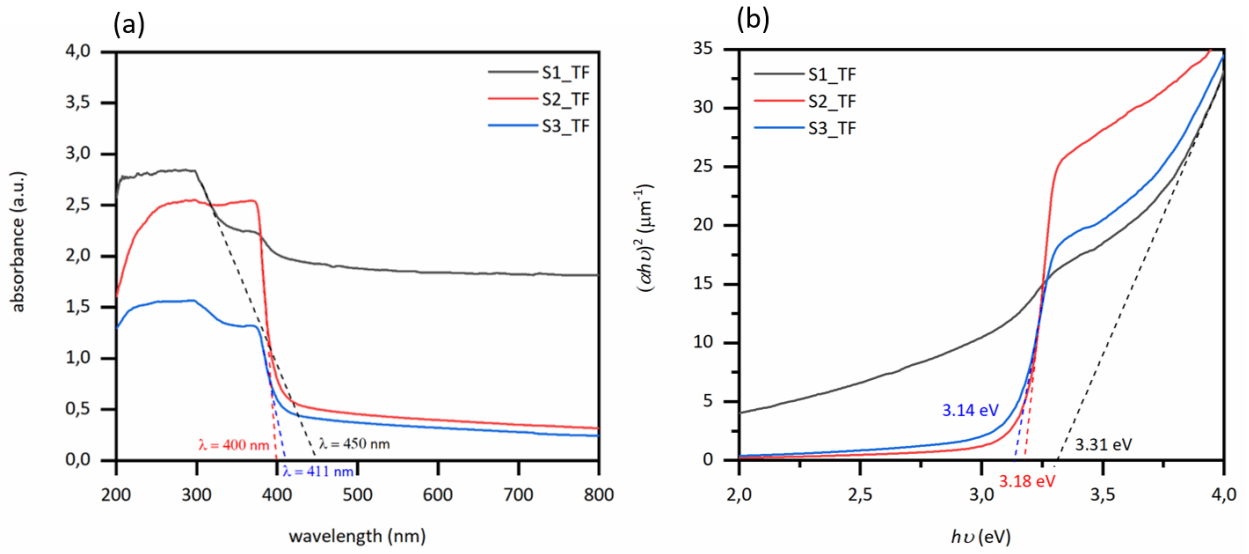

Figure 4. (a) Absorbance spectra and (b) Bandgap (Eg) of ZnO thin films annealed at different oxidation temperatures

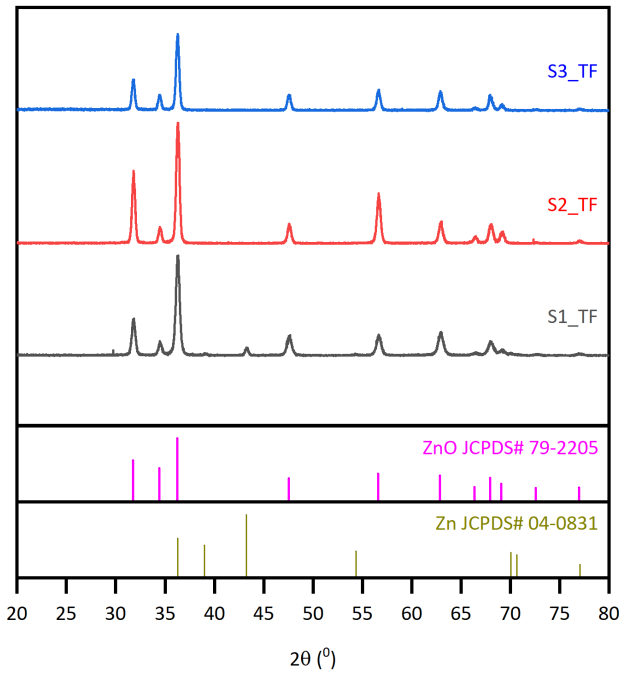

Figure 5. XRD patterns of the ZnO thin films annealed at different oxidation temperatures

In order to measure average crystallite size (D) of these ZnO thin films, well-known formula of Debye-Scherrer is used (2):

$$D = \frac{0.94\lambda}{\beta cos\theta} \quad (3)$$

Where β is the observed angular FWHM of the peak, λ is the X-ray wavelength (1.5406A° for Cu Ka_1) and θ is the Bragg's angle. Average crystallite size of all samples is shown in Table 1. From Table 1, FWHM value of all samples indicated that they have a good crystal quality of hexagonal structure, especially S3_TF that has smallest value of β compared to other samples [18]. Furthermore, average crystallite sizes of these films are proportional with the oxidation temperatures. This phenomena might originate from the presence of the immobilized free radicals on the surface of ZnO thin films, which later produce lattice contraction (1).

Table 1: Details information from XRD analysis for ZnO thin films annealed at different oxidation temperatures

No.	Sample	Oxidation Temp. (°C)	β(°)	β(rad)	2θ(°)	θ(°)	θ(rad)	D(nm)
1	S1_TF	450	0.4688	0.0082	36.29	18.145	0.3167	17.6608
2	S2_TF	550	0.3910	0.0068	36.30	18.150	0.3168	21.2969
3	S3_TF	650	0.3834	0.0067	36.27	18.135	0.3165	21.6147

The surface textures of the ZnO seed layer with different oxidation temperatures were studied by FESEM and shown in Figure 6. S1_TF, which is shown in Figure 6 (a) and (b), has thickness around 2.26 to 2.52 µm. However, it seems like some nanowires has grown up to 2.02 µm at the top of the thin film. From the top-view, these nanowires are grown as needle-like shape grains. In Figure 6 (c) and (d), these nanowires (S2_TF) were become lesser as the sample was oxidized at 550°C. The needle-like shape grains also start to merge with each other and become spherical-like shape grains. For S3_TF, no nanowires were found at the top of the thin film and its top-view is more agglomerate compare to S2_TF, as shown in Figure 6 (e) and (f). Moreover, these micrographs show that higher oxidation temperature will produce larger grains of ZnO thin film, which is supported by the XRD analysis. All ZnO seed layers are successfully fabricated by annealing process in the tube furnace and prepared for ZnO NRs growth process.

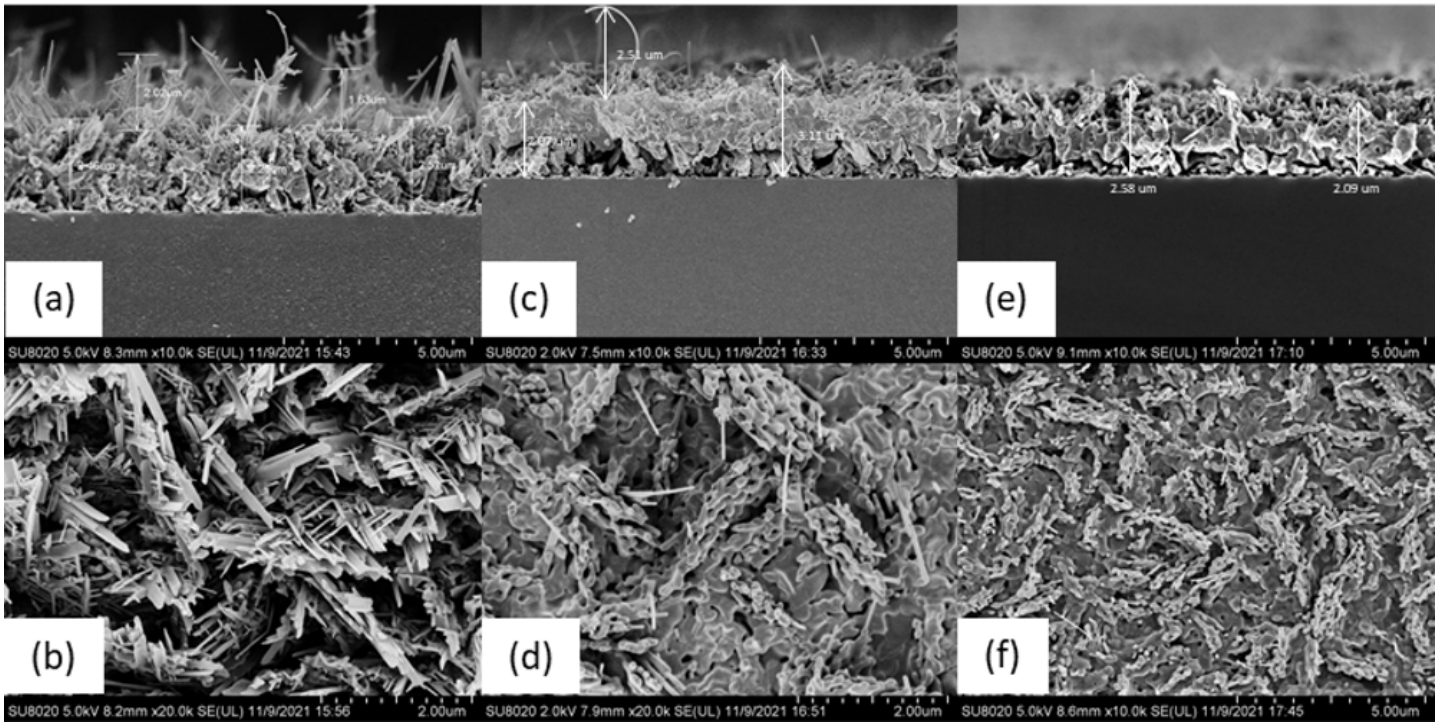

Figure 6. FESEM micrographs of S1_TF (a) and (b); S2_TF (c) and (d); S3_TF (e) and (f)

Optical, Structural and Morphological Analysis of ZnO NRs

UV-Vis-NIR Spectrometer was used for measuring the absorbance and energy bandgap of ZnO NRs samples. As shown in Figure 7 (a), ZnO NRs have strong optical absorption at the edge of ultraviolet range (~400 nm). This phenomenon may be attributed to O:2p – Zn:4s charge-transfer band [19]. Furthermore, sample S1_NR suddenly has lowest absorbance edge, unalike S1_TF. Subsequently, the absorbance edges for NRs samples are proportional with the oxidation temperature. Changes in absorbance edge of S1_TF and S1_NR might due to the 'lost' of unreacted Zn in S1_TF, which later affect the absorbance edge of S1_NR. Nevertheless, previous research found that pure ZnO NRs have an absorption edge in the range of 347 to 365 nm [20]. In our case, the absorption-edge of these ZnO

thin film samples have larger range of wavelength. Excess oxygen vacancies within the lattice may be the cause of this event to happen, besides, there are also more light scattering at the grain boundaries. Equation (1) was used to measure the energy bandgap of ZnO thin film samples, similar to ZnO thin films. X-axis intersections of a straight line plotted from the graph between $(\alpha h\upsilon)^2$ versus hu are the value of energy bandgaps, similar to bandgap analysis of ZnO thin film.

From Figure 7 (b), energy bandgap of S1 is reduced from 3.31eV (S1_TF) to 3.12 (S1_NR); S2 reduced from 3.18 eV (S2_TF) to 3.15 eV (S2_NR); and S3 reduced from 3.14 eV (S3_TF) to 3.08eV S3_NR). These reduction in bandgap values is caused by crystallinity improvement as the phase of thin film changes to NRs (1). Nevertheless, S1_NR energy bandgap became smallest value among these three samples. This event is related with its absorbance-edge analysis as explained before, and caused by disappearing unreacted Zn in the sample after the nanorods growth process by sol-gel immersion method.

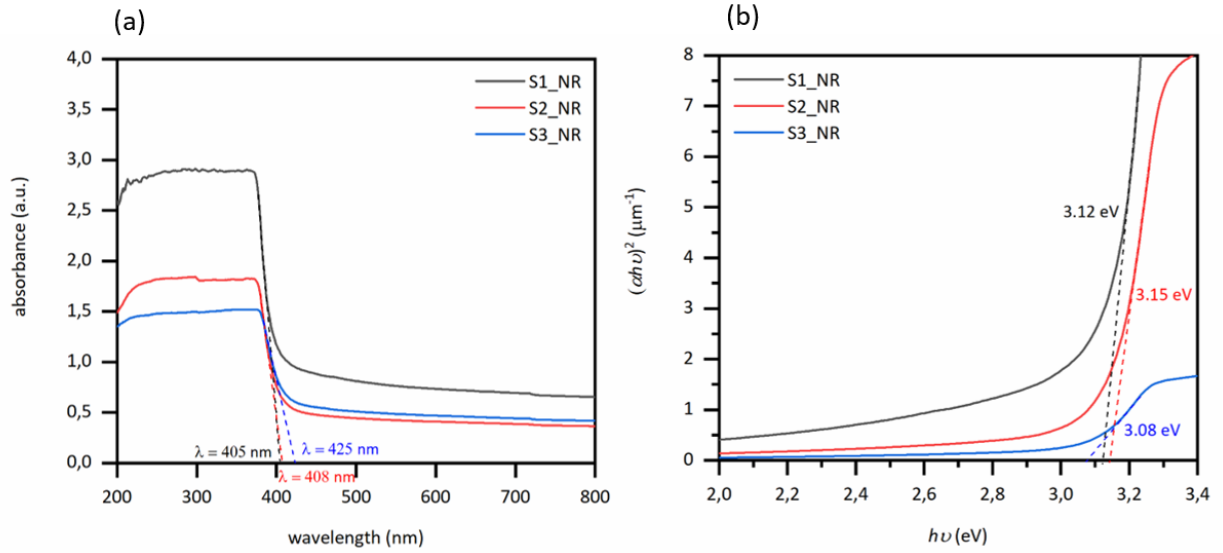

Figure 7. (a) Absorbance spectra and (b) Bandgap (Eg) of ZnO NRs annealed at different oxidation temperatures

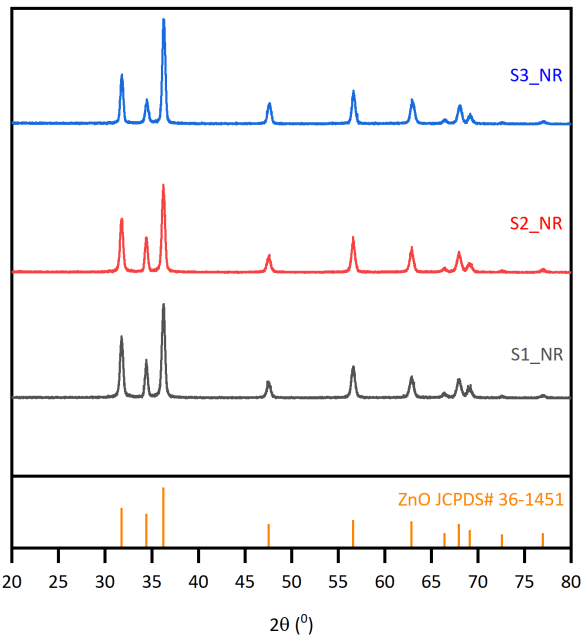

Figure 8. XRD patterns of S1_NR, S2_NR and S3_NR

For all ZnO nanorods (NR), peaks are found at 31.77° (100), 34.42° (002), 36.25° (101), 47.54° (102), 56.60° (110), 62.86° (103), 66.38° (200), 67.96° (112), 69.10° (201), 72.56° (004), 76.95° (202), correspond to JCPDS# 36-1451, as shown in Figure 8. Peak at 36.25° is the highest peak with planes (101), showing that the ZnO nanorods growth were highly crystalline although they are not vertically aligned. This is proven by FESEM micrographs, that will be showed later. Also shown in the XRD patterns, sample S1_NR has no Zn peaks found. It shows that Zn atoms that did not oxidized in S1_TF had already reacted with zinc nitrate hexahydrate and hexamethylenetetramine solution during nanorods growth process, and 'disappeared' from the sample, which is proportional with its optical analysis that explained before. Furthermore, from the XRD analysis, FWHM value for S1_NR, S2_NR and S3_NR are 0.4062°, 0.3850° and 0.3824°. These values are still inversely proportional to oxidation temperature, similar with XRD analysis for ZnO thin films. NRs samples have smaller FWHM value compared to their results at phase of thin films, caused by higher crystallinity of NRs (1).

Micrographs of ZnO NRs, captured by FESEM are shown in Figure 9. In Figure 9 (a) and (b), rods of S1_NR were formed on the SLG substrate. However, the sizes are quite large and reached size of micron. S2_NR has smaller size of microrods, yet are quite big to called nanorods, which can be seen in Figure 9 (c) and (d). Nevertheless, for S3_NR sample, as shown in Figure 9 (e) and (f), nanorods were successfully formed although they are not vertically aligned. In short, all NRs samples grew at (101) plane, as reported in XRD analysis. These FESEM investigations also determined that higher oxidation temperature will produce better ZnO NRs.

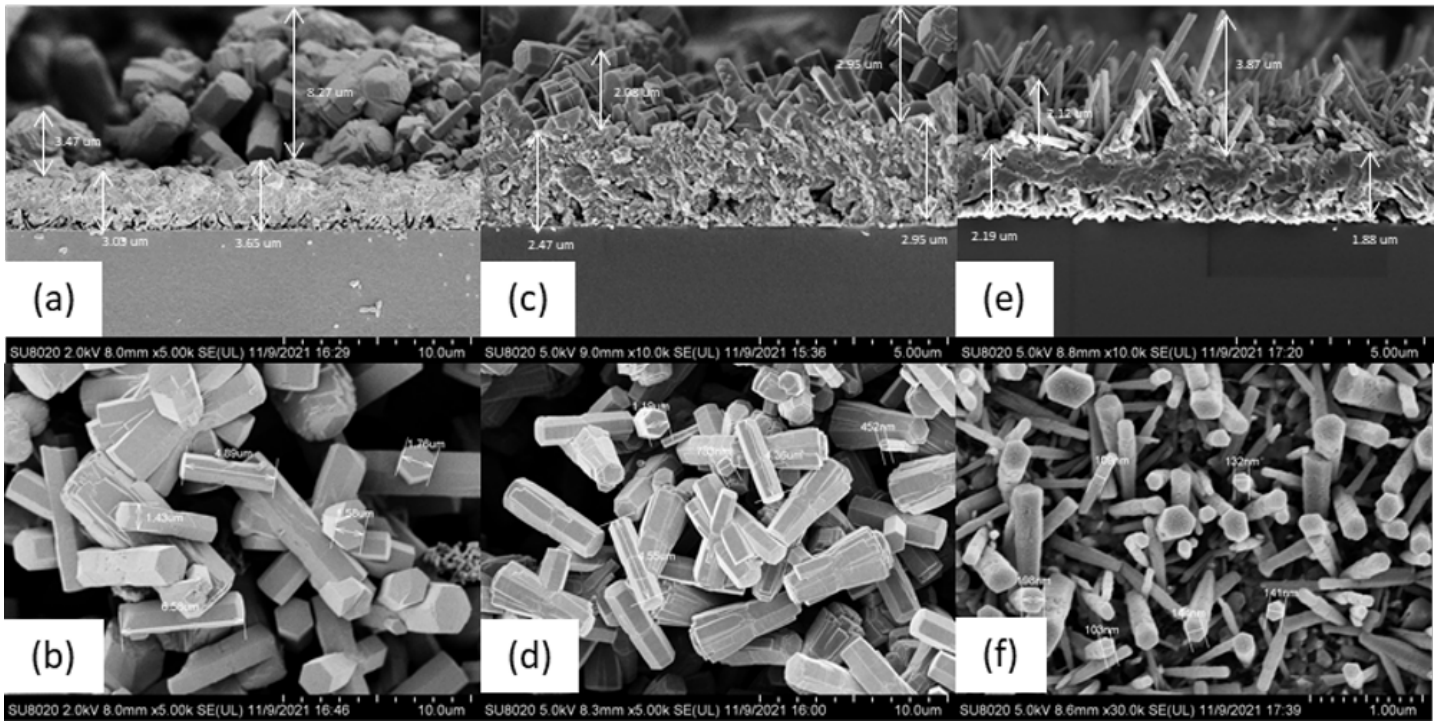

Figure 9. FESEM micrographs of S1_NR (a) and (b); S2_NR (c) and (d); S3_NR(e) and (f)

Conclusions

ZnO thin film layer was successfully deposited on SLG substrate by thermal evaporation method followed by post-annealing at different oxidation temperatures. Subsequently, ZnO NRs structures were grown on the surface of the seed layer by sol-gel immersion method utilizing 0.1 M zinc nitrate hexahydrate and 0.1 M HMT in DI water. XRD analysis shows that the ZnO NRs exhibit increasing peak intensity and decreasing FWHM values at (101) plane as temperature increases, indicating subsequent improvement in alignment and crystallinity of the sample. The optical band gap energy of ZnO NRs decreases in the range of 0.03 eV to 0.19 eV as compared to its 2D bulk ZnO film. This phenomenon could be assigned

to the optical confinement effect during the formation of ZnO NRs. Morphological analysis shows that the diameter of as-grown ZnO NRs decreased with increasing oxidation temperature, in which the average diameter was successfully recorded at 100 nm for the NRs grown at 650 ^{o}C for 3 hours. It is shown that the characteristic of the ZnO nanostructure could be improved by the pre-deposited ZnO seed layer as prepared at the different annealing temperatures. The findings will contribute towards increment in understanding and anticipation on further progress in 1D ZnO nanomaterial-based optoelectronic devices.

Conflicts of Interest

The author(s) declare(s) that there is no conflict of interest regarding the publication of this paper.

Acknowledgment

This work is financially supported by International Matching Grant between Universiti Teknologi Malaysia and Universitas Negeri Malang Indonesia with a cost center number of R.J130000.7354.4B685.

References

[1] Theerthagiri, J., S. Salla, R.A. Senthil, P. Nithyadharseni, A. Madankumar, P. Arunachalam, T. Maiyalagan and H.-S. Kim, *A review on ZnO nanostructured materials: energy, environmental and biological applications.* Nanotechnology, 2019. **30**(39): p. 392001.

[2] Sandeep, K.M., S. Bhat and S.M. Dharmaprakash, *Structural, optical, and LED characteristics of ZnO and Al doped ZnO thin films.* Journal of Physics and Chemistry of Solids, 2017. **104**: p. 36-44.

[3] Zahoor, R., A. Jalil, S.Z. Ilyas, S. Ahmed and A. Hassan, *Optoelectronic and solar cell applications of ZnO nanostructures.* Results in Surfaces and Interfaces, 2021. **2**: p. 100003.

[4] Antony, A., S. Pramodini, P. Poornesh, I.V. Kityk, A.O. Fedorchuk and G. Sanjeev, *Influence of electron beam irradiation on nonlinear optical properties of Al doped ZnO thin films for optoelectronic device applications in the cw laser regime.* Optical Materials, 2016. **62**: p. 64-71.

[5] Mahmoud, A., M. Echabaane, K. Omri, L. El Mir and R. Ben Chaabane, *Development of an impedimetric non enzymatic sensor based on ZnO and Cu doped ZnO nanoparticles for the detection of glucose.* Journal of Alloys and Compounds, 2019. **786**: p. 960-968.

[6] Drobek, M., J.-H. Kim, M. Bechelany, C. Vallicari, A. Julbe and S.S. Kim, *MOF-Based Membrane Encapsulated ZnO Nanowires for Enhanced Gas Sensor Selectivity.* ACS Applied Materials & Interfaces, 2016. **8**(13): p. 8323-8328.

[7] Taufiq, A., H.N. Ulya, C.I. Yogihati, Sunaryono, N. Hidayat, N. Mufti, Masruroh, S. Soda and T. Ishida, *Effects of ZnO nanoparticles on the antifungal performance of Fe3O4/ZnO nanocomposites prepared from natural sand.* Advances in Natural Sciences: Nanoscience and Nanotechnology, 2020. **11**(4): p. 045004.

[8] Yadollahi, M., I. Gholamali, H. Namazi and M. Aghazadeh, *Synthesis and characterization of antibacterial carboxymethyl cellulose/ZnO nanocomposite hydrogels.* International Journal of Biological Macromolecules, 2015. **74**: p. 136-141.

[9] Shetti, N.P., S.D. Bukkitgar, K.R. Reddy, C.V. Reddy and T.M. Aminabhavi, *ZnO-based nanostructured electrodes for electrochemical sensors and biosensors in biomedical applications.* Biosensors and Bioelectronics, 2019. **141**: p. 111417.

[10] Ding, M., Z. Guo, L. Zhou, X. Fang, L. Zhang, L. Zeng, L. Xie and H. Zhao, *One-Dimensional Zinc Oxide Nanomaterials for Application in High-Performance Advanced Optoelectronic Devices.* Crystals, 2018. **8**(5): p. 223.

[11] Ye, Z., T. Wang, S. Wu, X. Ji and Q. Zhang, *Na-doped ZnO nanorods fabricated by chemical vapor deposition and their optoelectrical properties.* Journal of Alloys and Compounds, 2017. **690**: p. 189-194.

[12] Thongsuksai, W., G. Panomsuwan and A. Rodchanarowan, *Fast and convenient growth of vertically aligned ZnO nanorods via microwave plasma-assisted thermal evaporation.* Materials Letters, 2018. **224**: p. 50-53.

[13] Laila, I.K.R., N. Mufti, S. Maryam, A. Fuad, A. Taufiq and Sunaryono, *Synthesis and Characterization of ZnO Nanorods by Hydrothermal Methods and Its Application on Perovskite Solar Cells.* Journal of Physics: Conference Series, 2018. **1093**: p. 012012.

[14] Di Mauro, A., M. Cantarella, G. Nicotra, V. Privitera and G. Impellizzeri, *Low temperature atomic layer deposition of ZnO: Applications in photocatalysis.* Applied Catalysis B: Environmental, 2016. **196**: p. 68-76.

[15] Ocakoglu, K., S.A. Mansour, S. Yildirimcan, A.A. Al-Ghamdi, F. El-Tantawy and F. Yakuphanoglu, *Microwave-assisted hydrothermal synthesis and characterization of ZnO nanorods.* Spectrochimica Acta Part A: Molecular and Biomolecular Spectroscopy, 2015. **148**: p. 362-368.

[16] Toe, M.Z., N.A.H.N. Jusoh, S.Y. Pung, K.A. Yaacob, A. Matsuda, W.K. Tan and S.S. Han, *Effect of ZnO Seed Layer on the Growth of ZnO Nanorods on Silicon Substrate.* Materials Today: Proceedings, 2019. **17**: p. 553-559.

[17] Mahendran, R., M. Kashif, D. Manickam, M. Venkatachalam, T. Kumar, A. Mariam, S. Chinnappanadar and U. Hashim, *Structural and optical characterization of ZnO thin films annealed at different temperatures.* Journal of Applied Sciences Research, 2013.

[18] Islam, M.S., M.F. Hossain, S.M.A. Razzak, M.M. Haque and M.N.I. Khan. *Zinc oxide thin film fabricated by thermal evaporation method for water splitting application*. in *2015 International Conference on Electrical & Electronic Engineering (ICEEE)*. 2015.

[19] Gill, R., S. Ghosh, A. Sharma, D. Kumar, V.-H. Nguyen, D.-V.N. Vo, T.-D. Pham and P. Kumar, *Vertically aligned ZnO nanorods for photoelectrochemical water splitting application.* Materials Letters, 2020. **277**: p. 128295.

[20] Salem, K.E., A.M. Mokhtar, I. Soliman, M. Ramadan, B.S. Shaheen and N.K. Allam, *Ge-doped ZnO nanorods grown on FTO for photoelectrochemical water splitting with exceptional photoconversion efficiency.* International Journal of Hydrogen Energy, 2021. **46**(1): p. 209-220.